Received: 21 December 2021 | Revised: 5 October 2022 | Accepted: 10 October 2022

DOI: 10.1111/fwb.14015

Freshwater Biology WILEY

ORIGINAL ARTICLE

Experimentation, modelling, and simulation of hydrochory in an Amazonian river

Ezequiel Barbosa da Silva[1] | Jonathan Luz Pires Crizanto[1] | Carlos Henrique Medeiros de Abreu[2,3] | Eldo Silva dos Santos[1,4] | Helenilza Ferreira Albuquerque Cunha[1,4,5] | Alaan Ubaiara Brito[5] | Gilvan Portela de Oliveira[6] | Leidiane Leão Oliveira[7] | Amanda Frederico Mortati[7] | Thiago André[7,8] | Jochen Schöngart[8] | Maria Teresa Fernandez Piedade[8,9] | Alan Cavalcanti da Cunha[1,2,5]

[1]Graduate Program in Tropical Biodiversity (PPGBIO), Federal University of Amapá (UNIFAP), Macapá, Amapá, Brazil

[2]Graduate Program in the Legal Amazon Biodiversity and Biotechnology Network (Bionorte), Macapá, Amapá, Brazil

[3]State University of Amapá, Brazil (UEAP) and PPG-Bionorte/UNIFAP, Macapá, Amapá, Brazil

[4]Environmental Science Course (CA), Federal University of Amapá, Macapá, Amapá, Brazil

[5]Graduate Program in Environmental Science (PPGCA), Federal University of Amapá (UNIFAP), Macapá, Amapá, Brazil

[6]Institute for Scientific and Technological Research of the State of Amapá–IEPA, Macapá, Amapá, Brazil

[7]Federal University of Western Pará – UFOPA, Santarém, Pará, Brazil

[8]Brasilia University – UnB, Manaus, Amazonas, Brazil

[9]National Institute for Amazonian Research, Amazonas (INPA), Manaus, Amazonas, Brazil

Correspondence
Alan Cavalcanti da Cunha, Graduate Program in Tropical Biodiversity (PPGBIO), Federal University of Amapá (UNIFAP), Macapá, Amapá, Brazil.
Email: alancunha@unifap.br

Funding information
CNPq, Grant/Award Number: 314830/2021-9, 441498/2017-5, 441481/2017-5, 441.462/2017-0, 441520/2017-0 and 309684/2018-8; DPq/PROPESPg/UNIFAP

Abstract

1. Seed transport by hydrochory is a key mechanism of long-distance dispersal constrained by attributes of the seed and hydrodynamics of the river, influenced by seasonal precipitation and hydrological pulses. However, the extent to which a hydrodynamic model can predict seed dispersal influenced by a tributary is unknown.
2. The study was conducted along a 10-km stretch of the Falsino River in Amapá, Brazil. Hydrodynamic parameters from the 2021 rainy season were used to calibrate a three-dimensional numerical model (SisBaHia) and simulate hydrochory of *Macrolobium bifolium*, a widely distributed species in the Amazon floodplains. This model was coupled with a Lagrangian dispersal model to estimate the average transport distance of the fruit plume. The simulated results were compared statistically with those of dispersal quantified in the field.
3. The field experiment coincided with the maximum hydrological pulse, providing with a maximum potential distance of longitudinal dispersal fruit of *c.* 10 km in 2 hr. The orders of magnitude of the mean plume transport (observed and numerically simulated centre of mass) were compatible with each other over six longitudinal tracking sections ($4.0\% \leq \text{estimated} \times \text{observed error} \leq 16.5\%$). Different channel stretches had distinct hydraulic characteristics that influenced spatial dispersal dynamics and are likely to be factors influencing the distribution of *M. bifolium* in these environments.
4. The present research is a contribution to understanding fluvial hydrodynamics and hydrochory by *M. bifolium*, whose seed dispersal syndrome is an adaptive characteristic that might explain its abundance and richness in these Amazonian riparian zones. We used *M. bifolium* as a model species to understand the role of seasonal flood pulse and fluvial hydrodynamics related to hydrochory favouring.

KEYWORDS
Amazon, Falsino River, long-distance dispersal, *Macrolobium bifolium*, National Forest of Amapá (FLONA-AP)

1 | INTRODUCTION

Seed dispersal is the transport process that generally offers higher success rates in establishment with increasing distance from the mother plant (Howe & Smallwood, 1982). This transport can occur by abiotic vectors such as water (hydrochory) and wind (anemochory) or biotic factors through animals (e.g., zoochory, ichthyochory). In addition to potentially expanding their distribution area, it facilitates gene flow regardless of whether it is high or low (da Cunha et al., 2017; Groves et al., 2009; Merritt & Wohl, 2006).

Water is one of the main means of propagule dispersal (seeds and fruits) in the densely vegetated riparian regions of the Amazon River floodplains (Kubitzki & Ziburski, 1994; Lopez, 2001; Parolin et al., 2013). An extensive hydrographic network favours this processes, with distinct hydrological pulses throughout the basin (Junk, 2005; Junk & Wantzen, 2004). The drainage network comprises large and medium-sized tributaries that perform a major role in the distribution of propagules over long distances (Dantas et al., 2021; Kubitzki & Ziburski, 1994; Scarano et al., 2003).

Hydrochory can occur along the longitudinal course of a river channel at the water's surface (air–water interface), in the water column, and in riverbeds (Carthey et al., 2016). In rivers of the Amazon basin, hydrochory is particularly common during the rainy season because monomodal and bimodal hydrological pulses play a relevant role in flooding (Junk, 2013). It is important to highlight that seeds and other propagules disperse by different mechanisms, varying with morphological traits that permit buoyancy. The density of floating seeds and propagules is lower than that of water, whereas, in the water column, their density is similar to that of water. Finally, on the riverbed, seeds and propagules usually roll or sink down to the channel bed, as their density is greater than that of water (Carthey et al., 2016). For instance, in the Amazon, *Carapa guianensis* seeds dispersal occurs on water's surface (Scarano et al., 2003). However, depending on the buoyancy stage, dispersal occurs also in the water column (Carthey et al., 2016). Most dispersal studies in the Amazon region emphasise dispersal by floating on the water's surface, e.g., *Hevea brasiliensis* (da Cunha et al., 2017; Moegenburg, 2002), although there are some records of species that disperse at the bottom of the river or with non-floating seeds (e.g., *Euterpe oleracea*; Moegenburg, 2002).

Many species use more than one form of dispersal, maximising their distribution within the nearby area. This is the case for *Macrolobium acaciifolium* (*Macrolobium bifolium*), which is dispersed by hydrochory (Kubitzki & Ziburski, 1994) and zoochory (Melo et al., 2019). Hydrochory is usually considered the main form of secondary dispersal in flooded environments (Pettit & Froend, 2001), and therefore, it seems the most relevant factor for species diversity in riparian habitats (Nilsson et al., 2010).

Given the complexity of Amazonian water systems, long-distance dispersal in large and medium-sized rivers is still challenging to quantify (Nathan et al., 2008). However, dispersal simulation models in Amazonian environments approximates dispersal distance, allowing for the comparison of empirical measurements with simulated scenarios in the short, medium, and even long term (da Cunha et al., 2017; Groves et al., 2009). Therefore, predictive numerical models can be helpful in studies of the complex hydrodynamic and dispersal behaviour of seeds in natural environments (Nathan & Muller-Landau, 2000). At this scale, the results can also promote new ecological strategies for the conservation of riparian populations. Such strategies rely on new studies to understand how the biotic and physical parameters involved interact with the dynamics of hydrochory in riparian ecosystems (Groves et al., 2009).

Fluvial transport of fruit (longitudinal, lateral, and transverse dispersal) can be described by the basic laws of physics (Navier–Stokes Equations; Abreu et al., 2020; da Cunha et al., 2021; Rosman, 2018). The pragmatic use of these equations in the study of dynamics of dispersal or hydrochory is a new and complex task, as it involves several factors that generate uncertainties about the hydrodynamics of the natural flow.

A second challenge in quantifying processes of hydrochory in medium and large rivers in the Amazon is the virtual absence of specific quantitative parameters and methods at this level or at the scale at which the phenomenon takes place. For example, the hydrology and hydraulics of many Amazon rivers are often poorly monitored. Given these limitations, understanding the role of fluid mechanics in natural Amazon River flows has been challenging (Abreu et al., 2020; da Cunha et al., 2021; Silva Dos Santos et al., 2018). To overcome the limitations in studies involving hydrochory, hydrodynamic and transport models (Lagrangian) should be coupled to describe this mechanism in nature. Finally, hydraulic characteristics of flow rates must also be inserted into the model (da Cunha et al., 2017).

Despite the importance of hydrochory in the Amazonian flooded forests, many studies assessing the distribution distance of propagules by hydrochory are carried out in marine systems or small rivers (Nilsson et al., 2010). In contrast, variation in longitudinal propagule dispersal is much less studied in freshwater systems, particularly in large and medium-sized rivers (da Cunha et al., 2017; Parolin et al., 2013). Furthermore, as the sub-basins of medium to large Amazonian rivers are extensive, and their tributaries may have varying hydrological regimes and flood levels, hydrochory occurs over large geographic scales with high spatial complexity (Junk et al., 2011; Less et al., 2021; Ward et al., 2013).

Given the scarcity of similar studies in the literature, the present study was carried out in the Falsino River basin, an oligotrophic blackwater river (igapó; Cunha, da Cunha, et al., 2013; Prance, 1980). The hydrological regime is monomodal, with a single annual pulse of

flooding and drought (Junk & Wantzen, 2004) and no tidal influence (Silva et al., 2020). The species chosen for the hydrochory experiments was *M. bifolium* (Aubl.) Pers. (Fabaceae), as it is abundant in the wetlands of the Amazon region (Lobo et al., 2019) and is widely distributed in the study area.

The goal of the present study was to investigate and describe the process of long-distance hydrochory of *M. bifolium* fruits and evaluate the influence of hydrodynamic parameters on a stretch of the Falsino River basin of approximately 10 km in length. In particular, we aimed to correlate observed data obtained in situ with the outputs of numerical simulation models.

2 | METHODS

2.1 | Study area

The Falsino River lies in the state of Amapá, northern Brazil (Figure 1a,b) within three Protected Areas (Figure 1c), occupying an area of 4,229 km^2 (Belúcio, 2020). The bathymetry and calibration data of the model were extracted from a 25-km length from the mouth of the Falsino River (Figure 1d), including the entire 10-km reach where the experimental study of hydrochory was carried out. The hydrodynamic and dispersal experiments started *c.* 200 m upstream of the MT16 section, extending to the MS11 section (Figure 1e). A census of *M. bifolium* was carried out along 20 km of the Falsino River, between the location of the ICMBio base (Chico Mendes Institute for Biodiversity Conservation) and a few kilometres upstream from the mouth of the Braço Creek. The Braço Creek is the main tributary of this stretch (right bank), and the Falsino River flows into the Araguari River (Figure 1d,e).

The predominant vegetation in the National Forest of Amapá (FLONA-AP) consists of tropical rainforest (ICMBIO, 2016) formed by a mosaic of *terra firme*, flooded forests of *igapó*, and cerrado (Simonian et al., 2003). Predominant soils in FLONA-AP are red-yellow oxisol, yellow oxisol, red-yellow podzolic soil, and petroplinthic soils (Belúcio, 2020; Camargo et al., 1987); the latter is also predominant in the studied region (ICMBIO, 2016). The rocks of FLONA-AP have a geomorphological origin that dates back to more than 1.6 billion years ago (IBGE, 2004), characterising the roughness of the riverbed and therefore considered in the bathymetric parameterisation of the numerical model (da Cunha et al., 2017). The region's climate is hot and humid (IBGE, 2002), with an average annual temperature between 25 and 26°C (ICMBIO, 2016). Total annual precipitation observed above the FLONA-AP canopy is approximately 2,181.2 mm, ranging between 70 mm/month in the dry period and 562.2 mm/month in the rainy period (Oliveira et al., 2020).

The study area is located between the coordinates 01°02′47.79″N–51°33′01.71″W and 01°02′41.76″N–51°32′34.98″W (Figure 1d). In addition to the experimental current measurements, bathymetry was carried out both in the Falsino River and in a short stretch near the mouth of the Braço Creek (Figure 1e) to measure and include the hydrodynamic effect of this tributary in the hydrochory simulation. We found that the Braço Creek contributes approximately 12% of the net discharge into the Falsino River (Figure 1e), whereas the net discharge of the Falsino River, on average, contributes approximately 32% to the flow of the Araguari River (March 2021; Figure 1d).

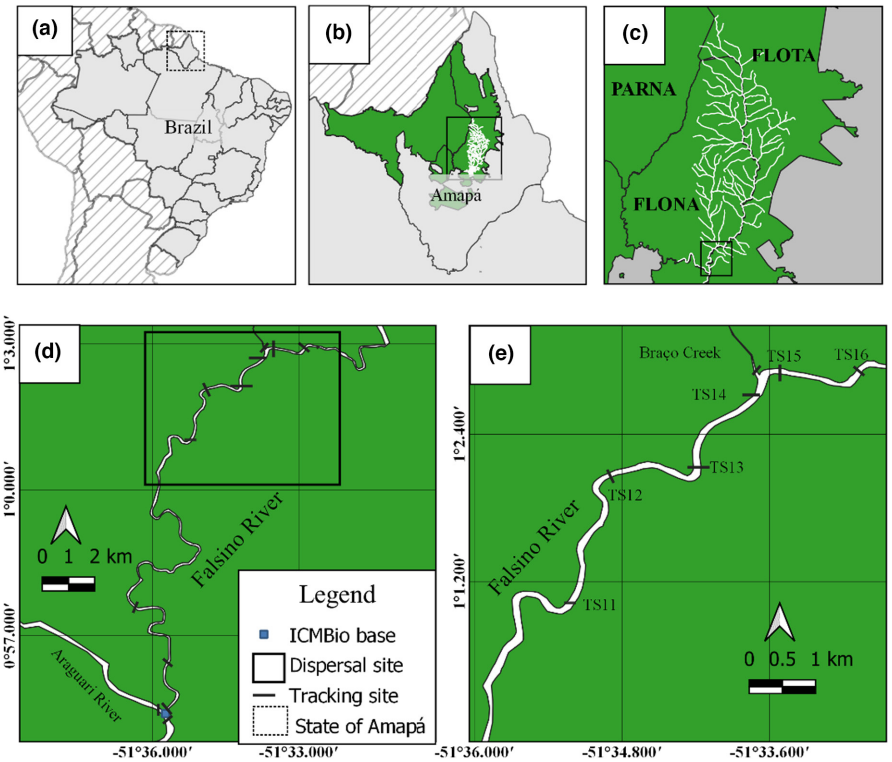

FIGURE 1 (a) Location of the State of Amapá in Brazil in South America; (b) localization of the study river within state of Amapá; (c) Falsino River basin in the central west of Amapá between three Protected Areas: Tumucumaque Mountains National Park (PARNA), National Forest of Amapá (FLONA), and State Forest of Amapá (FLOTA); (d) exclusive bathymetry (2018) and flow measurement sections for calibration (2021); (e) Specific stretch used in the hydrochory experiment coincident with the hydrodynamic measurement sections (10-km section), including the Braço Creek tributary. TS = sections measuring the flow values for model calibration

In the studied section of the Falsino River has a steep slope (s = 0.50%; Cunha, Cunha, & Pinheiro, 2013) and a predominantly rocky riverbed, with frequent alternating characteristics of turbulent rapids and calmer water, where reaches with wide or curved banks and accentuated meanders appear (Figure S2).

2.2 | Ecological characteristics of the studied species

Macrolobium bifolium (Aubl.) Pers. (Fabaceae) occurs in Amazonian floodplains, where it can be found in *campinarana* and *terra firme* environments (da Silva et al., 2017; Lorenzi, 2016; Martins-da-Silva & Lima, 2020; Targhetta et al., 2015). Campinarana is a type of vegetation in the Amazon region, with varied physiognomies, from grassland to forested. The species has a wide distribution, including the northern Brazilian states of Pará, Amapá, Amazonas, Acre, Rondônia, and Roraima (Martins-da-Silva & Lima, 2020). *Macrolobium bifolium* is popularly known as *iperana*, *ipê-da-várzea*, *ipê*, and *ipezeiro* (da Silva et al., 2017; Lorenzi, 2016). Its fruits are leguminous, dehiscent, woody, oblong to spatulate, and may contain one to three oval or orbicular seeds (da Silva et al., 2017; Feitoza et al., 2014), measuring on average 3.7 × 3.7 cm. The seeds are denser than water, as previously recorded for *M. acaciifolium* (Kubitzki & Ziburski, 1994); therefore, they depend on the fruit to be dispersed by floating. In the field, we observed that buoyancy occurs with the fruit open and closed. We did not discriminate this biological characteristic in the present study because, even during the experimental stage, its opening could occur naturally by explosion. Fruits for the experiment were collected directly from the trees of *M. bifolium* distributed along the lower Falsino River (Figure S3), which was previously inspected to avoid mouldy and damaged fruits. A total of 486 fruits were collected in 2021 and 219 in 2019. Their biometric measurements were taken soon after collection, with mean and standard deviation values as follows: length, 8.68 ± 1.10 cm; width, 5.26 ± 0.75 cm; thickness, 1.29 ± 0.19 cm; weight, 22.26 ± 0.60 g; density, 0.37 ± 0.09 g cm^3.

We adopted the centre of mass (CM) of the fruit plume to simplify comparative analysis between the average observed and numerical results and the impossibility of simultaneously tracking all the fruits dispersed in the river. We were able to apply the CM concept because the experimental duration was relatively short (10 km in 2 hr). In this interval, the plume of fruits dispersing in the current was visible to observers, so it was possible to track it. That is, visualisation of the plume centre and the natural spreading of fruits on the water surface was maintained for the longest possible period.

2.3 | Hydrodynamic data collection and field processing

Bathymetry data were obtained in August 2018. As the Falsino riverbed is predominantly rocky, we considered that the bottom bed remained geomorphologically unchanged when compared to the 2021 experiment. Flow data collections and calibrations of the hydrodynamic model were performed in March 2021. Maximum variation in the flood pulse amplitude occurs in the region during this period (March to May; Silva et al., 2020; Silva Dos Santos et al., 2018). In March, we also performed the dispersal experiment using the *M. bifolium* fruits, when the species has the highest fruit production rate (March–April), representing the most favourable period for hydrochory.

Bathymetric mapping and current measurement (hydrodynamics) were performed using an Acoustic Doppler Current Profiler (a 3 MHz ADCP/Surveyor M9 SonTek ADCP). The equipment has four 1-MHz transducers that are submerged at *c*. 0.5 m. Bathymetry was carried out along a 25-km stretch, from the mouth of the Falsino River to the upstream point TS01, passing through the mouth of the Braço Creek (TM01 in Figure 1c,d). Bathymetric data were recorded using River Surveyor Live software associated with ADCP and a GPS (Garmin 76CSx). Sampled stretches of the 25 km of the river had an average depth (h) of 5.46 m, an average width (W) of 78.48 m, and an average aspect ratio of W/h *c*. 15 (Figure S2) in most sections. Bathymetric survey data were generated by Kriging over an 831 finite element grid using Google Earth® version 6.1.0.5001 (Google, Inc.), Surfer® version 10.1.561, 64-bit (Golden Software, Inc.), and Argus ONE® version 4.2.0q (Argus Holdings Ltd.).

Flow measurements were replicated three times using the ADCP in each of the six tracking cross-sections of the Falsino River and its tributary Braço Creek (Figure S2). The measurements were considered valid when the relative errors between each of them were less than 5%. These procedures enabled generating a three-dimensional (3D) map (geometric parameter of the hydrodynamic model of the natural channel bed), from which the model's initial and boundary conditions were then established. Flow data were entered as physical parameters of the longitudinal sections of the hydrodynamic model domain for calibration purposes. The hydrodynamic calibration process allowed generating the mean simulated flow, from which we could compare the maximum simulated and observed distances in time and in each section monitored in the field. This was done to compare the mean CM transport distance between the simulated and observed scattered fruits as well as identify and quantify the maximum errors (E_{Max}).

2.4 | Fruit dispersal field experiment

In March 2021, 486 fruits were launched directly and simultaneously into the centre of the channel at precisely the DFA01 point (initial launch point), approximately 500 m upstream of section TS16 (Figure 3d). After fruit launching, the average transport rate of CM—where they were most concentrated—was monitored in space and time using GPS by two observers present in two boats following the plume, one upstream of the plume CM and the other downstream of it. This experimental process lasted for at least

2 hr, reaching a total transport distance of approximately 10 km, at sampling intervals of *c*. 10 min to record the position of the plume CM. As the fruits presented a somewhat asymmetrical distribution, with a shorter tail upstream and a longer tail downstream of the maximum seed peak, we considered that the CM was located approximately one-third of the distance from the front of the plume (Figure S1). Interval measurements of the CM transport created a spatiotemporal record of the plume and its comparison with measurements of the hydrodynamic numerical calibrated simulation model (da Cunha et al., 2017).

The first boat stayed an average distance of 20 m upstream from the first seed of the plume to avoid hydrodynamic interference in the currents. The second boat was an average distance of 20 m downstream of the posterior tail of the plume (last visible seed). To avoid the considerable difficulties of visualising the plume in moving water, where it reached up to 1.0 m/s (or greater than 1.0 m/s) in several stretches, we added small portions of biodegradable starch powder (similar to popcorn) to the fruits. We found that this powder helped visualise the plume yet at no time interfered with the dispersal movement of the fruits. After seed tracking, the results for times and distances of experimental and simulated transport of the plume CM were statistically compared and correlated (da Cunha et al., 2017; Rosman, 2018).

2.5 | Modelling and simulation of hydrochory

The information included in the dispersal model was defined to parameterise the model and generate the experimental scenario of seed dispersal measured in the field and computationally. It was then necessary to include the 3D physical properties of flow, location, and start/end time (da Cunha et al., 2017). Average liquid discharge (Q *c*. 500 m/s) and average current speed (v_c *c*. 1.0 m/s) were measured in the six sections. Average wind speed (v_w < 0.5 m/s) was estimated based on the only existing meteorological station (Porto Grande), located 65 km away from the launch point. Thus, Q, v_c, and v_w were the main parameters used in simulation of the dispersal process (Abreu et al., 2020; Cunha et al., 2012; da Cunha et al., 2021; Rosman, 2018).

The entire modelling process was performed using SisBaHia software (http://sisbahia.coppe.ufrj.br/; Rosman, 2016), an open-access modelling platform developed by Fundação Coppetec of the Federal University of Rio de Janeiro, Rio de Janeiro, Brazil. SisBaHia comprises a Filtered In Space and Time (FIST) hydrodynamic model optimised for natural waterbodies, water quality models, and Eulerian and Lagrangian transport models of transport phenomena (Rosman, 2016). The FIST3D model (3D version of the FIST hydrodynamic model) solves the complete Navier–Stokes equations (Equations 1–3). Figure 2 represents a total flow profile so that the 3D phenomenon can be represented in the 2DH format to facilitate generation of velocity and dispersal fields at each iteration of the numerical simulation (Rosman, 2018).

Prediction of the dispersal process was made using a Lagrangian model of advection–diffusion for seed transport. The objective was to identify the effects of natural channel hydrodynamics on the maximum potential distances of seed dispersal (CM) during the hydrological process of the rainy season in the Falsino River (March 2021), according to Equations 1, 2, and 3, as follows:

$$\frac{\partial \zeta}{\partial t}+\frac{\partial UH}{Ux}+\frac{\partial VH}{\partial y}=\Sigma q \tag{1}$$

$$\frac{\partial U}{\partial t}+U\frac{\partial U}{Ux}+V\frac{\partial U}{\partial y}=-g\frac{\partial \zeta}{\partial x}-\frac{gH}{2\rho_\circ}\frac{\partial \hat{\rho}}{\partial x}+\frac{1}{H\rho_\circ}\left(\frac{\partial\left(H\hat{\tau}_{xx}\right)}{\partial x}+\frac{\partial\left(H\hat{\tau}_{xy}\right)}{\partial y}\right)+\frac{1}{H\rho_\circ}\left(\tau_x^S-\tau_x^B\right)-\frac{1}{H\rho_\circ}\left(\frac{\partial S_{xx}}{\partial x}+\frac{\partial S_{xy}}{\partial y}\right)+2\Phi\text{sen}V-\frac{U}{H}\Sigma q \tag{2}$$

$$\frac{\partial V}{\partial t}+U\frac{\partial V}{Ux}+V\frac{\partial V}{\partial y}=-g\frac{\partial \zeta}{\partial y}-\frac{gH}{2\rho_\circ}\frac{\partial \hat{\rho}}{\partial x}+\frac{1}{H\rho_\circ}\left(\frac{\partial\left(H\hat{\tau}_{xy}\right)}{\partial x}+\frac{\partial\left(H\hat{\tau}_{xy}\right)}{\partial y}\right)+\frac{1}{H\rho_\circ}\left(\tau_y^S-\tau_y^B\right)-\frac{1}{H\rho_\circ}\left(\frac{\partial S_{yy}}{\partial y}+\frac{\partial S_{xy}}{\partial x}\right)-2\Phi\text{sen}U-\frac{V}{H}\Sigma q \tag{3}$$

where *U* is the velocity on the axis *x* (m/s); *V* is the velocity on the axis *y* (m/s); ζ represents the free elevation of the water surface (m); *H* is the depth of the water column (m); ρ_o is the average density of water (kg/m^3); ρ_r is the reference density of water (kg/m^3); *g* is the acceleration of gravity (m/s^2); τ_{ij} is the turbulent tension tensor; (*i*, *j*) are indices on the horizontal plane (*x*; *y*); $\tau_y^S - \tau_y^B$ are the wind tension on the water surface minus the lowest frictional tension, respectively (kg m^{-1} s^{-2}); $2\Phi sen\theta U$ and $2\Phi\theta senV$ represent the Coriolis accelerations; Φ is the angular velocity of the Earth's rotation (rad/s); θ is the latitude angle; $\sum q$

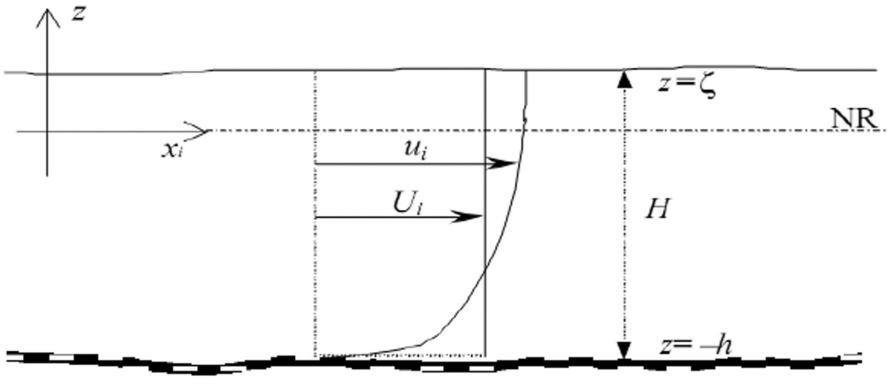

FIGURE 2 Three-dimensional (2DH) graphical representation. Model coordinates are shown, where NR represents the water reference level. U_i is the vertically integrated velocity; u_i is the velocity of the 3D (2DH) model, which varies with depth; ξ is the elevation of the free surface of the water, and *h* is the depth obtained by bathymetry; *H* is the instantaneous depth ($H = \xi + h$; adapted from Rosman, 2018)

represents the water balance based on atmospheric precipitation, infiltration, and evaporation; S_{ij} represents the effect of radiation tensions (Cunha & Brasil Junior, 2006; Rosman, 2018).

The 3D (or 2DH) hydrodynamic model considers the incompressible water flow and constant water density at the control volume of the moving fluid. The dispersing sources in the Lagrangian model are represented by several particles launched in the region (DFA01) at a single instant of time ($P^n = 0$ min). Particles randomly arranged in the region of origin are transported by currents, calculated using the hydrodynamic model. The position of any particle at the next instant is defined by P^{n+1}, approximated by an expansion of the second-order Taylor series, based on the previously known prior position of the particles (P^n; Equation 4):

$$P^{n+1} = P^n + \Delta t \frac{dP^n}{dt} + \frac{\Delta t^2}{2!} \frac{d^2P^n}{dt^2} + O^3 \quad (4)$$

Regarding the passive agent in the natural flow (propagules) from any source (in this case, DF01), the amount of mass (M_a) of a particular species observed in each particle when entering the modelled domain is given by Equation 5:

$$M_a = \frac{qs\, C_a \times \Delta \tau}{N_P} \quad (5)$$

The flow q_s is the instantaneous seed discharge from the source (m^3/s), C_a is the seed concentration found from the source discharge (kg/m^3), and N_P is the number of particles (fruits) that enter the domain through the source at time interval $\Delta t(s)$. The dimensions of the mass source region are defined so that the seed source is observed at the end of the initial dilution process within the mixing field near the plume (Abreu et al., 2020; da Cunha et al., 2021; Rosman, 2018).

The total flow measured by the ADCP in each river section is the result of integrating four measurements performed automatically: (1) water column or surface flow (within 0.5 m of the water–air interface); (2) right bank flow (operator-defined); (3) left bank flow (operator-defined); and (4) bottom flow, estimated automatically by the ADCP. Interpolations and extrapolations of surface, sides, and bottom were performed using a logarithmic model (Mueller et al., 2009). The total flow integrated into each section was quantified for hydrodynamic analysis and subsequent numerical model calibration. The mean water level was obtained from experimental ADCP values during in situ measurements of the flow in the six sections along the 25-km study area (Figure 1e and Figure S2). However, the exclusive experimentation and modelling of hydrochory took place on only a 10-km stretch from the seed launching point (DAF01).

2.6 | Parameterization of the hydrodynamic model

The input data were spatially distinguished on an 831 finite element grid (3D map: bathymetry). The defined parameters in the finite element domain for applying Equations 1–5 of the hydrodynamic model included amplitude of riverbed roughness, riverbank slope, and flow conditions (Q). The riverbed was considered rough as it is moderately low in clay content and has sand and many rocks. The roughness of the riverbed was considered constant (0.001) in all elements of the grid. A normal flow condition was assumed for elements along the smooth sloping riverbanks (near 45°). This assumption was made because it was not computationally possible to include irregular riverbanks or other debris (trunks, roots, vegetation, and others).

A previous sensitivity analysis of the model was performed, varying the parameters that defined the roughness of the riverbed and the slope of the riverbanks within realistic ranges. Error estimates were verified concerning adherence of observed data to model limitations. The objective was to evaluate model performance; for this purpose, a correlation coefficient between the observed and modelled data was also used.

2.7 | Simulation of fruit dispersal (Lagrangian model)

Dispersal of floating seeds on the water surface was simulated based on the hydrodynamic model (Equations 1–3) and the Lagrangian numerical model coupled with the hydrodynamic model. The purpose was to represent the movement of fruits as closely as possible to the reality in the current (Equations 4 and 5). The Lagrangian model was selected because it can be applied efficiently to problems with instantaneous point sources or in other similar investigations (da Cunha et al., 2017). The hydrodynamic model was calibrated according to local hydrodynamic characteristics. We later simulated the transport of the plume based on the calibrated hydrodynamic model.

It is important to mention that some fruits were trapped along the riverbanks due to the vegetation characteristics of the edges or near the Braço Creek tributary (Figure 1e), which did not occur with the simulated plume. For this reason, the focus of the hydrochory analyses was the plume CM and not the individual fruits. However, average distances between the experimental and simulated CMs were statistically tested to assess the model's effectiveness in representing the average hydrochory phenomenon.

3 | RESULTS

3.1 | Observed dynamics of hydrochory

Flow values to calibrate the model are shown in Table 1, and their respective transversal profiles are represented in Figure S2. The comparison of observed and simulated flows showed variations with relative error values between 0.7% and 10%. Thus, the low relative error values enabled model calibration and application of linear regression tests between the observed and simulated transport

TABLE 1 Comparative hydrodynamic parameters for transport of experimental and simulated centres of mass (CMs) of plumes dispersed by hydrochory

Section	Dispersal time (min)	CM experimental distance (km) from L0	Simulated CM distance (km) from L0	Absolute difference between CM distances (km)	Relative error (%) – Distance	Experimental average speed (m/s)	Simulated average speed (m/s)	Relative error (%) – speed	Experimental flow (m^3/s)	Simulated flow (m^3/s)	Relative error (%) – flow
DFA01*	10	0.85	0.71	0.14	16.57	1.25	1.19	16.57	454	468	−3.08
DFA02*	20	1.64	1.49	0.14	8.64	1.18	1.25	8.64	445	473	−6.29
DFA03*	30	2.25	2.05	0.20	9.10	1.04	1.14	9.10	513	558	−8.77
DFA04	40	3.09	2.75	0.35	11.42	1.47	1.14	11.42	–	–	
DFA05*	50	3.86	3.43	0.42	10.89	1.31	1.15	10.89	545	541	0.73
DFA06	60	4.73	4.30	0.43	9.18	1.25	1.19	9.18	–	–	
DFA07	70	5.53	4.92	0.61	11.03	1.39	1.17	11.03	–	–	
DFA08*	80	6.22	5.84	0.37	6.08	1.11	1.22	6.08	540	510	5.55
DFA09	90	7.04	6.21	0.82	11.73	1.13	1.15	11.73	–	–	
DFA10*	100	8.02	7.24	0.77	9.65	1.38	1.21	9.65	511	564	−10.37
DFA11	110	8.66	7.98	0.68	7.90	0.86	1.21	7.90	–	–	
DFA12	120	9.51	8.88	0.62	6.55	1.39	1.23	6.55	–	–	
DFA13*	130	10.1	9.77	0.48	4.72	1.15	1.24	4.72	–	–	

Note: Sections are shown in Figure 3e.

Abbreviations: CM, centre of mass; DFA01*, flow measurement in the MT16 area; DFA02*, flow measurement in the MT15 area; DFA03, flow measurement in area S14; DFA05, flow measurement in the MT13 area; DFA08, flow measurement in the MT12 area; DFA10, flow measurement in the MT11 area.

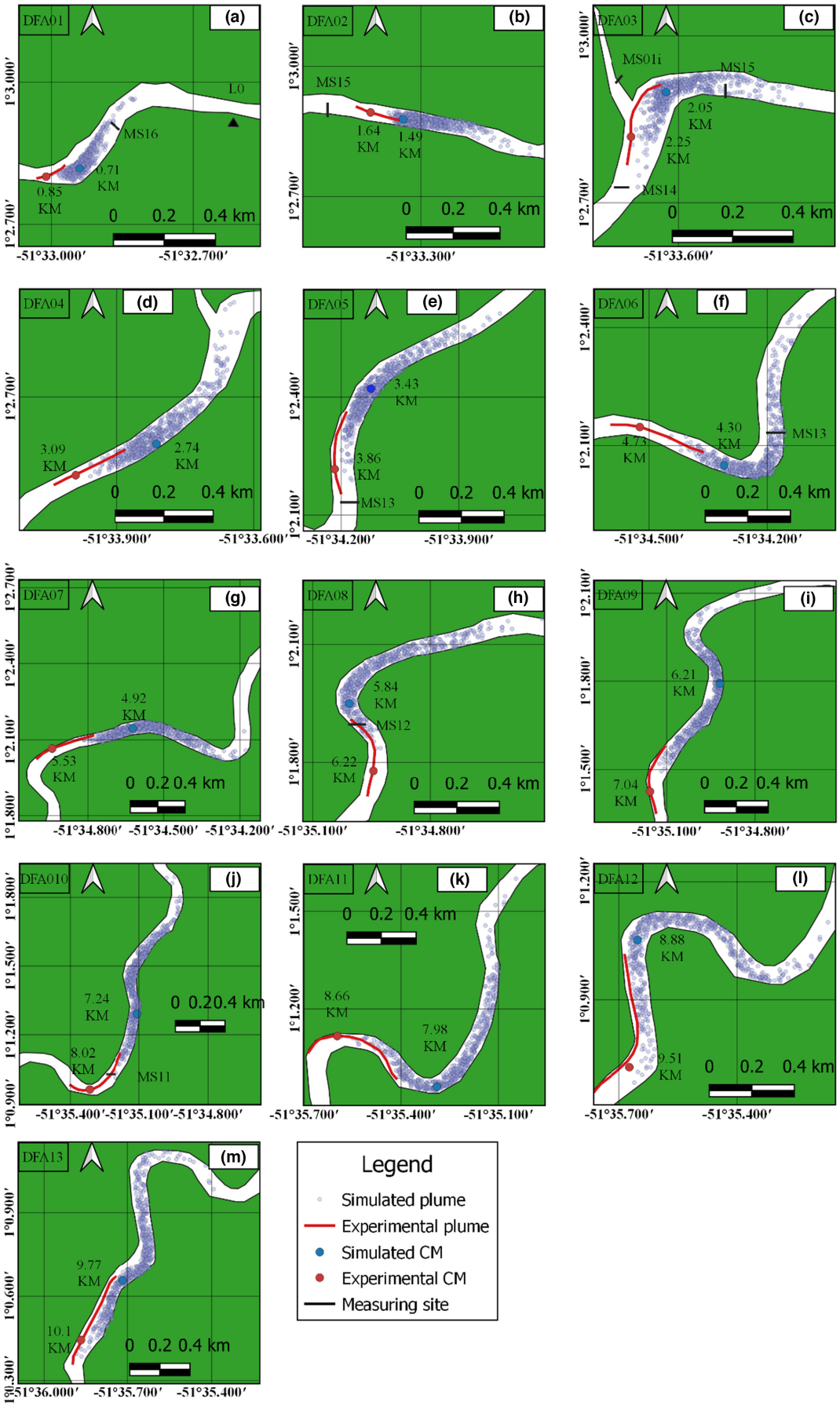
DFA01
(a)
L0
MS16
0.71 KM
0.85 KM
0 0.2 0.4 km
1°3.000′
1°2.700′
-51°33.000′
-51°32.700′
DFA02
(b)
MS15
1.64 KM
1.49 KM
0 0.2 0.4 km
1°3.000′
1°2.700′
-51°33.300′
DFA03
(c)
MS01i
MS15
2.05 KM
2.25 KM
MS14
0 0.2 0.4 km
1°3.000′
1°2.700′
-51°33.600′
DFA04
(d)
3.09 KM
2.74 KM
0 0.2 0.4 km
1°2.700′
-51°33.900′
-51°33.600′
DFA05
(e)
3.43 KM
3.86 KM
MS13
0 0.2 0.4 km
1°2.400′
1°2.100′
-51°34.200′
-51°33.900′
DFA06
(f)
4.30 KM
4.75 KM
MS13
0 0.2 0.4 km
1°2.400′
1°2.100′
-51°34.500′
-51°34.200′
DFA07
(g)
4.92 KM
5.53 KM
0 0.2 0.4 km
1°2.700′
1°2.400′
1°2.100′
1°1.800′
-51°34.800′
-51°34.500′
-51°34.200′
DFA08
(h)
5.84 KM
MS12
6.22 KM
0 0.2 0.4 km
1°2.100′
1°1.800′
-51°35.100′
-51°34.800′
DFA09
(i)
6.21 KM
7.04 KM
0 0.2 0.4 km
1°2.100′
1°1.800′
1°1.500′
-51°35.100′
-51°34.800′
DFA010
(j)
7.24 KM
8.02 KM
MS11
0 0.20.4 km
1°1.800′
1°1.500′
1°1.200′
1°0.900′
-51°35.400′
-51°35.100′
-51°34.800′
DFA11
(k)
0 0.2 0.4 km
8.66 KM
7.98 KM
1°1.500′
1°1.200′
-51°35.700′
-51°35.400′
-51°35.100′
DFA12
(l)
8.88 KM
9.51 KM
0 0.2 0.4 km
1°1.200′
1°0.900′
-51°35.700′
-51°35.400′
DFA13
(m)
9.77 KM
10.1 KM
0 0.2 0.4 km
1°0.900′
1°0.600′
1°0.300′
-51°36.000′
-51°35.700′
-51°35.400′
Legend
Simulated plume
Experimental plume
Simulated CM
Experimental CM
Measuring site

FIGURE 3 (a–m) Sequence of DFA maps in the Falsino River (dispersal of the centres of mass, CM) showing the dispersal of *Macrolobium bifolium* fruits with 13 observations carried out in 2021. Sections DFA01, DFA02, DFA03, DFA04, DF05, DFA06, DFA07, DFA08, DFA09, DFA10, DFA11, DFA12, and DFA13. The red line represents the length of the experimental plume (experimental CM). The blue dots represent the simulated plume (simulated CM) in space and time. MS indicates the measurement section, and L_0 represents the initial moment of dispersal (seed launching).

distance of the plumes' CM. Statistically, the coefficient of determination between them was *c.* 99%. This correlation confirms the hypothesis that the CM chosen at 1/3, 1/2, or 2/3 of the longitudinal distribution of the plume was independent for the present case. Therefore, it is possible to consider the location of CM at 1/3 as a suitable position for purposes of comparing it with the experimental plume along the experimental measurement path or time interval (i.e., a likely position of most seeds in the discharge—CM), as well as with observations in the field.

3.2 | Simulation of hydrochory (Lagrangian model)

Field observations resulted in approximately 2 hr of experimental tracking of *M. bifolium* fruits. The experimental CM travelled 10 km in those 2 hr, although, on average, the experimental CM moved faster than the simulated CM (Figure 3a–m, Table 1) at all time intervals. During the 2-hr tracking of *M. bifolium* fruits, *c.* 25% of the total fruit visually observable was lost. However, fruit loss was not registered in the numerical simulation, which included smooth edges without drifts or losses.

In section DFA01, the CM of the experimental and simulated plumes were 0.85 and 0.71 km away from the reference point, respectively, represented by the launch point (L0 initial instant). In section DFA02, the transport of the observed and simulated CMs was more than 1 km from the launch point. For both sections, DFA01 and DFA02, there were no significant differences between the transport of the experimental and simulated CMs, where the absolute difference was 0.14 km between the two sections (Table 1 and Table S1, and Figure 3a,b). The average experimental speed in sections DFA01 and DFA02 was 1.25 and 1.18 m/s, respectively.

From section DFA03 (Figure 3c) onward, the fruits began to show greater variation between the distances covered by the observed and simulated CMs, with an absolute difference of 0.20 km between them. In this regard, the distance between the observed and simulated CMs was 2.25 km, when the plumes were already 2.05 km away from the launch point (DFA01). However, the average speed in this stretch was 1.04 m/s for the observed CM, a lower value than that of the previous measurement.

In sections DFA4, DFA5, DFA6, and DFA7 (Figure 3), there was another trend in the difference between the transport distance of observed and simulated CMs (Table 1). This difference was reduced in DFA08, while it increased in DFA09 (Table 1). From DFA09 onward, the difference in the distance between the CMs again diminished until the end of the experiment (10 km away from launch point L_0). Therefore, from the initial moment, the differences between the distances covered by the observed and simulated CMs showed a gradual growth trend (Table 1), stabilising only in the final sections.

Section DFA11, representing the widest stretch of the channel, had the lowest recorded mean speed. However, the observed speed throughout the trajectory was between 0.86 and 1.47 m/s. Consequently, the average length of the plumes varied in all sections. Table S1 also shows the longitudinal development of the experimental and simulated plume along the trajectory. The simulated length variation corresponded to the behaviour of the observed CM. The longitudinal dispersal steps of the observed and simulated plumes showed good physical correspondence of current acceleration and deceleration. Between DFA01–DFA06 and DFA08–DFA13, the plumes maintained their physically similar and coherent behaviour along their trajectories.

4 | DISCUSSION

The dispersal of germinative propagules in floodplain regions is marked by adaptations to seasonality in the Amazon Basin (Kubitzki & Ziburski, 1994). The dispersal process of *M. bifolium* resembles that of *Hevea spruceana*, *Ormosia excelsa*, and *Cecropia latiloba*. These species have a dry fruit at the initial dispersal stage, which starts with its *explosion* from the mother tree via dehiscence and senescence (autochory). However, *M. bifolium* depends exclusively on one of the pericarps to continue hydrochory because the density of the isolated seed is higher than that of water (>1.00 g/cm^3). The present biometric analyses of the seeded fruits showed a mean density value of 0.37 g/cm^3, similar to that of fruits dispersing over long distances in the Amazon basin, such as *Carapa guianensis* (da Cunha et al., 2017; Scarano et al., 2003).

The average flow of the Falsino River in the rainy season, measured experimentally, provides favourable conditions for propagule dispersal over long distances. In this matter, the biometrics of the fruit favours the dispersal process of the propagules (Carthey et al., 2016), as some can float for hours or days, as is the case of *Laetia suaveolens*, whose buoyancy occurs at intervals of up to 24 hr and *Mora paraenses*, which can float for over 100 days (Kubitzki & Ziburski, 1994). Nevertheless, although specific data on the buoyancy of *M. bifolium* fruits are not yet available, it is possible to infer that its buoyancy time surpasses 14 days, for both open and closed fruits.

In the present study, all fruits floated during the experiment. Given the speed of river current, we can affirm that some fruits could easily reach the mouth of the Falsino River and follow the Araguari River in 6 hr. Furthermore, within approximately 2 days of dispersal, some of these fruits could surpass the river's mouth and

reach the Cachoeira Caldeirão Hydroelectric Power Plant, which is *c*. 60 km downstream from the mouth of the Falsino River on the Araguari River. However, it is worth noting that this process does not occur at greater distances as the number of propagules tends to decline (natural reduction in the number of fruits and seeds) along this distance (Nathan et al., 2008).

We estimated a loss of approximately 25% of the fruits during the 2 hr of the experiment, where we observed that some of them dispersed laterally, travelling by different velocities of the longitudinal current (or side winds). The fruits eventually travelled at velocities greater than average, and, consequently, were distanced from the field observer. This same challenge in tracking propagules from long distances occurs due to the dynamic processes to which the propagules are subjected, generating losses of fruits throughout the experiment (Nilsson et al., 2010). However, throughout the numerical simulation of *M. bifolium*, the number of fruits was conservatively estimated for convenience. Experimentally, fruits are lost in the runoff, whereas they are not in a simulation. For these reasons only, the CM focus on mass rather than each individual particle was used for the dispersal comparison. Therefore, we used the concept of dispersal plumes to represent the overall process of hydrochory.

Nonetheless, this conservative estimate of distance travelled did not seem to impact the average errors of numerical outputs since the main dispersal focus is the plume CM and not the units. For instance, in the present study, the relative errors of transport of the experimental and simulated CMs were relatively low (Table 1), near to or lower than the results found by da Cunha et al. (2017), ranging from 4.8% to 13%. Schurr et al. (2008) highlight that these errors are common in predictive models due to the physical complexity involved in dispersal events. However, models have successfully explained the average dispersal behaviour of their studied CMs, facilitating the understanding of how to realistically vary the length of the dispersal core and the motion of the particles within the computational domain.

The model was a very good representation of the average travel behaviour of the CMS, as indicated by the high correlation between observed and simulated dispersal ($R^2 = 99\%$). High values of R^2 (98%) were also found by Groves et al. (2009), who studied hydrochory of sunflower seeds in the Wingecarribee River, Australia. In that case, the river's width and depth were less than that of the Falsino River. A relatively short experimental time interval is recommended because similar results also seem to occur in simulated hypothetical pollutant plumes in the Araguari River (Cunha, Cunha, & Pinheiro, 2013).

An interesting aspect of the dispersal process is that the simulated CM transport showed a greater difference starting in the DFA03 section, probably influenced by the lateral forces of the discharge from the Braço Creek. Such behaviour was also registered in previous studies (Shaheed et al., 2021; Weber et al., 2001), which demonstrate the influence of tributaries in the seed dispersal by water. Furthermore, local geomorphology is important in the generation of secondary currents (helical flows). Although this phenomenon is little studied, it is very common in rivers with intense currents and accentuated curvatures or close to meanders that tend to alter, even imperceptibly, the lateral dispersal behaviour of the propagules at these critical flow points (Santos & Cunha, 2021).

We detected a characteristic hydrodynamic behaviour through almost the entire route, that is, an *oscillation* in the longitudinal length of the plume, both observed and simulated. This same oscillation was also found in studies simulating pollutant dispersal in the Araguari (Cunha, Cunha, & Pinheiro, 2013) and Amazon rivers, where these variations are likely to be related to bathymetric uncertainties and bottom roughness (Abreu et al., 2020). In other words, these variations might be related to irregular riverbed geometry not captured during bathymetric quantification or where the river is wider and deeper and probably serve as an additional and potential source of errors in quantifying natural flow. In addition, vertical and lateral recirculation can occur. For instance, in section DFA9, the transport distances between simulated and experimental CM increased again. However, from section DFA10 to section DFA13, the CM was reapproached due to a gradual increase in the simulated speed compared to the observed one. These results are in line with Merritt and Wohl (2006), who claimed that the hydrodynamics determines the spatial patterns of processes of hydrochory, many of which are influenced by the bathymetric profile of the river (Abreu et al., 2020; da Cunha et al., 2017; Santos & Cunha, 2021). The characteristic of speed variation (or seasonal flow) is a fundamental factor in hydrochory for *M. bifolium* and must be considered a key parameter of the spatial distribution of riparian species.

The spatial distribution of adult *M. bifolium* trees along the studied stretches of the Falsino River appeared to have a pattern coinciding with some of the hydraulic characteristics observed throughout the 25-km stretch studied (curves, straight lines, meanders, presence, or absence of a tributary). For instance, we observed a greater concentration of *M. bifolium* trees in places closer to the mouth of the Falsino River. In these sites, the number of mother plants increases on both banks when the river becomes wider and closer to the mouth, particularly in stretches with more accentuated curves or with meanders. The distribution of trees observed along both banks seems to correspond to the hydraulic characteristics of the natural channel (reduction of current velocity and channel widening). Thus, near the mouth of the river, there are more opportunities for lateral dispersion where the velocity is lower, and, usually, the fruits are more sensitive to the effects of sides wind or secondary flow currents (helical current effect). The helical effect is a combination of the average effect of the intensities of the main (longitudinal) and secondary (side or recirculating) currents (da Cunha et al., 2017; Santos & Cunha, 2021). This physical interaction may accentuate or induce transverse movements of the fruits in wider and more curvilinear stretches, which are areas with a greater tendency to accumulate fruits.

Secondary currents, mainly in medium and large rivers such as the Araguari and Maracá in Amapá (da Cunha et al., 2017; Santos & Cunha, 2021), can present a helical behaviour in relation to the longitudinal flow. Their role is relevant in Amazon rivers because secondary currents induce transverse circulation in relation to the main longitudinal flow, which can be intensified or inhibited by tributaries

(Santos & Cunha, 2021). Such hydrodynamic behaviour can also induce the formation of seed *deposits* precisely in those areas close to meanders and curves, as with the transport of sediments by water in general (Santos et al., 2014).

It is not possible to consider only a single trend or physical variable responsible for the likely distribution of fruits and seeds along the waterbody, as other environmental variables can contribute to this complex distribution and diversity of plants along the riverbank or tributaries (Shi et al., 2020). For instance, flooded (riparian) areas are governed by several other environmental variables, including the amplitude of the flood pulse (Junk, 2005), channel slope (Shi et al., 2020), precipitation (Oliveira et al., 2020), flood regime (Lucas et al., 2013), presence of anoxic soils (Belúcio, 2020; Wittmann et al., 2006), sediment granulometry and margins (Shi et al., 2020), flow turbulence level (Shi et al., 2020), liquid discharge and flow speed at critical points in the flow (da Cunha et al., 2017), luminosity influenced by the width between margins (Lucas et al., 2013), and original distribution of species along the margins of the waterbody (de Jager et al., 2019).

Detailed hydrodynamic modelling studies with a numerical simulation approach to hydrochory are still scarce in the literature, especially with regard to the Amazon (da Cunha et al., 2017). To our knowledge, this is the first investigation carried out in the Amazon region that involves hydrodynamic physical parameters with analysis of the influence of a tributary on seed dispersal, which uses the hydrodynamic approach to study riparian zones of *igapós* within protected areas (FLONA-AP). Despite the methodological challenges in the field, there are significant advantages to the use of hydrodynamic modelling to assess seed dispersal in medium and large rivers. In addition, the same methodology can be used for similar quantifications with other species of plants or trees with the same seed dispersal syndrome if it is possible to quantify the relevant hydrodynamic parameters in the field. Thus, once the numerical models are hydrodynamically calibrated, similar studies can be carried out with other species are also dispersed by hydrochory. Experimental costs only justify the studies of species relevant to conservation of floodplain and *igapó* ecosystems representative of the Amazon riparian zones (da Cunha et al., 2017).

Understanding hydrochory in the Amazon region is critical, mainly for the conservation of endangered riparian species in these tropical ecosystems (Dantas et al., 2021; de Jager et al., 2019; Feitoza et al., 2014; Groves et al., 2009; Lobo et al., 2019; Lucas et al., 2013; Merritt & Wohl, 2006). Hydrological anomalies influenced by extreme events, caused by climate change, such as drought and floods have been increasingly more frequent in rivers and lakes in the eastern Amazon estuary (Cunha & Sternberg, 2018). The implications these hydrological changes for hydrochory are as yet unknown.

At the global level, rivers and streams represent <0.6% of the Earth's land surface but play a disproportionately larger role, such as in biogeochemical cycles, providing locally relevant ecosystem services (Tagestad et al., 2021). The influence of rivers on material balances and ecosystem services remains largely unknown due to the lack of specific studies. Some Amazonian riparian zones may experience significant variations in hydrological processes such as extreme droughts (that are already present in many basins, including the Araguari River; Cunha & Sternberg, 2018; Silva Dos Santos et al., 2018) could jeopardise the adaptation and resilience of endemic tropical riparian species, especially those that disperse by hydrochory (Nathan et al., 2008; Nathan & Muller-Landau, 2000). Therefore, even without considering the effects of direct anthropogenic changes to river flows (i.e. dams), changes in hydrological processes will be potentially catastrophic for dispersal processes (Silva et al., 2020; Nilsson et al., 2002). For these reasons, hydrodynamic modelling and simulation emerge as a promising tool. For instance, the Falsino River flows into the Araguari River, which has also been experiencing a number of environmental impacts on potentially endangered species. This river has a series of three large hydroelectric dams (Silva et al., 2020) that act as a physical barrier hindering the natural movement of seeds and fruits over long distances, with unpredictable consequences downstream. Therefore, dams on the Araguari River may function as physical filters that inhibit hydrochory. Furthermore, near the mouth of the Falsino River, it was observed that flow decreased rather than increasing as expected. This may be due to the hydraulic influence of a dam located downstream on the Araguari River (Cachoeira Calderião Hydroelectric Power Plant), it is possible that long waves reflected by the dam can propagate against the natural flow, forming a hydraulic backwater in a significant stretch of the Falsino River mouth (up to 2–3 km), precisely where we recorded the largest number of mother plants of *M. bifolium*.

This scenario presents considerable challenges for the conservation of riparian ecosystems, mainly for hydrochoric dispersal by key species (such as *M. bifolium*). Thus, we perceive the strong dependence of the dispersal process on the hydrological and hydrodynamic characteristics of waterbodies. However, these hydrological parameters are generally poorly known and monitored in the Amazon region.

Our findings contribute to understanding of the ecology of river floodplains. Despite the promising results from the simulated dispersal model, differences inherent in the modelling process were found. Moreover, these discrepancies often occur because it is not possible to precisely represent the physical environment by models. In this study, the simulation underestimated the distance travelled by the fruit plume observed in the field. The relevant factors explaining such differences were probably due to imperfections in the bathymetric analysis (roughness, presence of obstacles in the margins not considered in the model, and others) and errors in current measurements in the field interfering with model hydrodynamic calibration (da Cunha et al., 2017). Besides that, the wind may have contributed significantly to the difference between the results observed in the field and the simulation ones because wind speed variable held constant in the model. For instance, wind tends to flow preferentially along the longitudinal corridors of the streams following the topography of the local channel and the morphology of the riparian crowns (Groves et al., 2009; Parolin et al., 2013; Shaheed et al., 2021; Shi et al., 2020). This fact may partly explain why the observed plume flowed faster than the simulated plume.

Despite these limitations, our integrated approach is still advantageous compared to purely empirical experiments observed in the literature because it allows us to make approximate estimates of dispersal over long distances using only hydraulic or hydrodynamic parameters that are readily measurable (bathymetry, speed, and flow). These parameters are usually sufficient to address the complexity of hydrochory in natural riparian environments like the one analysed in this study.

5 | CONCLUSION

This study represents an important advance in the characterisation of hydrochory and seasonal flow of a medium-sized river in the Amazon basin, although an understanding of fruit or seed dispersal is crucial for planning and management for biodiversity conservation, due to its influence on gene flow, diversity, and ecosystem function, the hydrodynamics involved are not well understood in these riparian ecosystems. Therefore, simulation models are important tools to address the complexity of the hydrochory. Our integrated approach, based on experimentation and modelling, adequately represented the average behaviour of the local process of hydrochory, with relatively low errors in contrast to the complexity of the flow and average transport of the CM of the experimental and model plumes (4.0 % < $Error_{[observed\text{-}model]}$ < 16%).

AUTHOR CONTRIBUTION

Conceptualisation: E.B.S., C.H.M.A., A.C.C. Developing methods: E.B.S., C.H.M.A., A.C.C. Conducting the research: E.B.S., J.L.P.C., C.H.M.A., E.S.S., H.F.A.C., A.U.B., G.P.O., L.L.O., A.F.M., T.A., J.S., M.T.F.P., A.C.C. Data analysis: J.L.P.C., C.H.M.A., E.S.S., A.U.B., A.F.M., T.A., J.S., M.T.F.P., A.C.C. Preparation of figures and tables: E.B.S., C.H.M.A., J.L.P.C., A.U.B., H.F.A.C., A.C.C. Data interpretation: E.B.S., C.H.M.A., A.F.M., T.A., J.S., M.T.F.P., A.C.C. Writing: E.B.S., C.H.M.A., J.L.P.C., E.S.S., H.F.A.C., A.U.B., G.P.O., L.L.O., A.F.M., T.A., J.S., M.T.F.P., A.C.C.

ACKNOWLEDGMENTS

We thank the Laboratory of Chemistry, Sanitation and Environmental Systems Modelling (LQSMSA), Laboratory of Hydraulic and Environmental Sanitation (Civil Engineering), as well as the National Council for Scientific and Technological Development (CNPq grants/processes: 309684/2018-8; 441520/2017-0; 441.462/2017-0; 441481/2017-5; 441498/2017-5), (Riparian Networks Project) and CNPq grant: 314830/2021-9 (Hydrodynamcs Networks Project) for support. Thanks also to DPq/PROPESPg/UNIFAP. We thank all ICMBio managers, directors, and agents for their unconditional support during the logistical and hosting stage at the Flona-AP base during the experimental studies.

DATA AVAILABILITY STATEMENT

The data are available from the corresponding author upon reasonable request.

ORCID

Ezequiel Barbosa da Silva https://orcid.org/0000-0003-2869-262X
Carlos Henrique Medeiros de Abreu https://orcid.org/0000-0003-0904-8791
Eldo Silva dos Santos https://orcid.org/0000-0001-6886-6298
Helenilza Ferreira Albuquerque Cunha https://orcid.org/0000-0001-7101-9305
Alaan Ubaiara Brito https://orcid.org/0000-0002-3850-2298
Amanda Frederico Mortati https://orcid.org/0000-0001-9150-990X
Thiago André https://orcid.org/0000-0003-4148-3662
Jochen Schöngart https://orcid.org/0000-0002-7696-9657
Maria Teresa Fernandez Piedade https://orcid.org/0000-0002-7320-0498
Alan Cavalcanti da Cunha https://orcid.org/0000-0002-1846-9486

REFERENCES

Abreu, C. H. M., Barros, M. d. L. C., Brito, D. C., Teixeira, M. R., & da Cunha, A. C. (2020). Hydrodynamic modeling and simulation of water residence time in the estuary of the Lower Amazon River. *Water*, *12*, 660. https://doi.org/10.3390/w12030660

Belúcio, L. P. (2020). *Pulso Hidrológico e gradientes edáfico-hidrográficos em paisagens ripárias mazônicas*. Universidade Federal do Amapá.

Camargo, M. N., Klamt, E., & Kauffman, J. H. (1987). *Classificação de solos usada em levantamentos pedológicos no Brasil*. EMBRAPA-SNLCS.

Carthey, A. J. R., Fryirs, K. A., Ralph, T. J., Bu, H., & Leishman, M. R. (2016). How seed traits predict floating times: A biophysical process model for hydrochorous seed transport behaviour in fluvial systems. *Freshwater Biology*, *61*, 19–31. https://doi.org/10.1111/fwb.12672

Cunha, A., & Brasil Junior, A. C. (2006). Numerical study of the surface flow in Matapi river mouth – internal stuarine Amapá coast. Curitiba.

Cunha, A., Brito, D., Brasil, J. A., Pinheiro, A., Cunha, H., Santos, E., & Krusche, A. V. (2012). Challenges and solutions for hydrodynamic and water quality in rivers in the Amazon Basin. In Hydrodynamics – Natural Water Bodies.

Cunha, A., Cunha, H., & Pinheiro, A. (2013). Modelagem e simulaçao do escoamento e dispersão sazonais de agentes passivos no Rio Araguari AP: Cenários para o AHE Ferreira Gomes-I-Amapá/Brasil. *Revista Brasileira de Recursos Hídricos*, *18*, 67–85. https://doi.org/10.21168/rbrh.v18n1.p67-85

Cunha, A. C., & Sternberg, L. d. S. L. (2018). Using stable isotopes 18O and 2H of lake water and biogeochemical analysis to identify factors affecting water quality in four estuarine Amazonian shallow lakes. *Hydrological Processes*, *32*, 1188–1201. https://doi.org/10.1002/hyp.11462

Cunha, E. D. d. S., da Cunha, A. C., da Silveira, A. M., Jr., & Faustino, S. M. M. (2013). Phytoplankton of two rivers in the eastern Amazon: Characterization of biodiversity and new occurrences. *Acta Botânica Brasílica*, *27*, 364–377. https://doi.org/10.1590/S0102-33062013000200011

da Cunha, A. C., De Abreu, C. H. M., Crizanto, J. L. P., Cunha, H. F. A., Brito, A. U., & Pereira, N. N. (2021). Modeling pollutant dispersion scenarios in high vessel-traffic areas of the Lower Amazon River. *Marine Pollution Bulletin*, *168*, 112404. https://doi.org/10.1016/j.marpolbul.2021.112404

da Cunha, A. C., & dos Santos, E. S. (2021). Circulação secundária atípica em meandro fluviomarinho como parâmetro hidrodinâmico em ecossistema aquático amazônico. *Revista Ibero-Americana de Ciências Ambientais*, *12*, 1–17.

da Cunha, A. C., Mustin, K., dos Santos, E. S., dos Santos, É. W. G., Guedes, M. C., Cunha, H. F. A., Rosman, P. C. C., & da Silveira Lobo Sternberg, L. (2017). Hydrodynamics and seed dispersal in the lower Amazon. *Freshwater Biology*, *62*, 1721–1729. https://doi.org/10.1111/fwb.12982

da Silva, M. M. F., Bastos, M. d. N. d. C., & Gurgel, E. S. C. (2017). O gênero Macrolobium Schreb. (Leguminosae) no estado do Amapá, Brasil. *Iheringia, Série Botânica*, *72*, 267–275.

Dantas, A. R., Guedes, M. C., da Cruz Vasconcelos, C., Isacksson, J. G. L., Pastana, D. N. B., Lira-Guedes, A. C., & Piedade, M. T. F. (2021). Morfologia, germinacion y distribucion geografica de *Pentaclethra macroloba* (Fabaceae): Arbol amazonico hiperdominante. *Revista de Biología Tropical*, *69*, 181–197.

de Jager, M., Kaphingst, B., Janse, E. L., Buisman, R., Rinzema, S. G. T., & Soons, M. B. (2019). Seed size regulates plant dispersal distances in flowing water. *Journal of Ecology*, *107*, 307–317. https://doi.org/10.1111/1365-2745.13054

Feitoza, G. V., dos Santos, J. U. M., Gurgel, E. S. C., & Oliveira, D. M. T. (2014). Morphology of fruits, seeds, seedlings and saplings of three species of *Macrolobium* Schreb. (Leguminosae, Caesalpinioideae) in the Brazilian Amazon floodplain. *Acta Botânica Brasílica*, *28*, 422–433. https://doi.org/10.1590/0102-33062014abb3341

Groves, J. H., Williams, D. G., Caley, P., Norris, R. H., & Caitcheon, G. (2009). Modelling of floating seed dispersal in a fluvial environment. *River Research and Applications*, *25*, 582–592. https://doi.org/10.1002/rra.1229

Howe, H. F., & Smallwood, J. (1982). Ecology of seed dispersal. *Annual Review of Ecology and Systematics*, *13*, 201–228. https://doi.org/10.1146/annurev.es.13.110182.001221

IBGE. (2002). Instituto Brasileiro de Geografia e Estatistica - informacoes ambientais/climatologia.

IBGE. (2004). Instituto Brasileiro de Geografia e Estatistica - informacoes ambientais/geologia.

ICMBIO. (2016). *Plano de Manejo da Floresta Nacional do Amapá – Diagnóstico*. Instituto Chico Mendes de Conservação da Biodiversidade (org.), Macapá, AP.

Junk. (2013). Brazilian wetlands: Their definition, delineation, and classification for research, sustainable management, and protection.

Junk, W. J. (2005). Flood pulsing and the linkages between terrestrial, aquatic, and wetland systems. *SIL Proceedings*, *1922–2010*, *29*, 11–38. https://doi.org/10.1080/03680770.2005.11901972

Junk, W. J., Piedade, M. T. F., Schöngart, J., Cohn-Haft, M., Adeney, J. M., & Wittmann, F. (2011). A classification of major naturally-occurring Amazonian lowland wetlands. *Wetlands*, *31*, 623–640. https://doi.org/10.1007/s13157-011-0190-7

Junk, W. J., & Wantzen, K. (2004). The flood pulse concept: New aspects, approaches and applications—An update. In: *Proceedings of the Second International Symposium on the Management of Large Rivers for Fisheries (LARS2)*.

Kubitzki, K., & Ziburski, A. (1994). Seed dispersal in flood plain forests of Amazonia. *Biotropica*, *26*, 30–43. https://doi.org/10.2307/2389108

Less, D. F. S., Ward, N. D., Richey, J. E., & Da Cunha, A. C. (2021). Seasonal and daily variation of hydrodynamic conditions in the Amazon River mouth: Influence of discharge and tide on flow velocity. *Journal of Coastal Research*, *37*(6), 1181–1192. https://doi.org/10.2112/JCOASTRES-D-21-00010.1

Lobo, G. d. S., Wittmann, F., & Piedade, M. T. F. (2019). Response of black-water floodplain (igapó) forests to flood pulse regulation in a dammed Amazonian river. *Forest Ecology and Management*, *434*, 110–118. https://doi.org/10.1016/j.foreco.2018.12.001

Lopez, O. R. (2001). Seed flotation and postflooding germination in tropical terra firme and seasonally flooded forest species. *Functional Ecology*, *15*, 763–771. https://doi.org/10.1046/j.0269-8463.2001.00586.x

Lorenzi, H. (2016). *Árvores Brasileiras. Manual de identificação e cultivo de plantas arbóreas nativas do Brasil – Volume 3, Edição: 2ª*. Plantarum.

Lucas, C. M., Bruna, E. M., & Nascimento, C. M. N. (2013). Seedling co-tolerance of multiple stressors in a disturbed tropical floodplain forest. *Ecosphere*, *4*, art3. https://doi.org/10.1890/ES12-00287.1

Martins-da-Silva, R. C. V., & Lima, H. C. (2020). Macrolobium in Lista de Espécies da Flora do Brasil. *Jardim Botânico do Rio de Janeiro*.

Melo, T., Torrente-Vilara, G., & Röpke, C. (2019). Flipped reducetarianism: A vegan fish subordinated to carnivory by suppression of the flooded forest in the Amazon. *Forest Ecology and Management*, *435*, 138–143. https://doi.org/10.1016/j.foreco.2018.12.050

Merritt, D. M., & Wohl, E. E. (2006). Plant dispersal along rivers fragmented by dams. *River Research and Applications*, *22*, 1–26. https://doi.org/10.1002/rra.890

Moegenburg, S. M. (2002). Spatial and temporal variation in hydrochory in Amazonian floodplain forest1. *Biotropica*, *34*, 606–612.

Mueller, D. S., & Wagner, C. R. (2009). Measuring discharge with acoustic Doppler current pro filers from a moving boat. *United States Geological Survey Methods*, *72*, https://doi.org/10.3133/tm3A22

Nathan, R., & Muller-Landau, H. C. (2000). Spatial patterns of seed dispersal, their determinants and consequences for recruitment. *Trends in Ecology & Evolution*, *15*, 278–285. https://doi.org/10.1016/S0169-5347(00)01874-7

Nathan, R., Schurr, F. M., Spiegel, O., Steinitz, O., Trakhtenbrot, A., & Tsoar, A. (2008). Mechanisms of long-distance seed dispersal. *Trends in Ecology & Evolution*, *23*, 638–647. https://doi.org/10.1016/j.tree.2008.08.003

Nilsson, C., Brown, R. L., Jansson, R., & Merritt, D. M. (2010). The role of hydrochory in structuring riparian and wetland vegetation. *Biological Reviews of the Cambridge Philosophical Society*, *85*, 837–858. https://doi.org/10.1111/j.1469-185X.2010.00129.x

Nilsson, C., Elisabet, A., Merritt, D., & Johansson, M. (2002). Differences in riparian flora between riverbanks and river lakeshores explained by dispersal traits. *Ecology*, *83*, 2878–2887.

Oliveira, L., Canani, L. G., Barreto, N., & Cunha, A. (2020). Hydric ecosystem services in a non-disturbed rainforest of the Amazon, Amapá, Brazil. *Nature Conservation*, *13*, 45–54. https://doi.org/10.6008/CBPC2318-2881.2020.004.0006

Parolin, P., Wittmann, F., & Ferreira, L. (2013). Fruit and seed dispersal in Amazonian floodplain trees – A review. *Ecotropica*, *19*, 19–36.

Pettit, N. E., & Froend, R. H. (2001). Availability of seed for recruitment of riparian vegetation: A comparison of a tropical and a temperate river ecosystem in Australia. *Australian Journal of Botany*, *49*, 515–528. https://doi.org/10.1071/bt00059

Prance, G. T. (1980). A terminologia dos tipos de florestas amazônicas sujeitas a inundação. *Acta Amazonica*, *10*, 499–504. https://doi.org/10.1590/1809-43921980103499

Rosman, P. C. C. (2016). Referência tecnica do SisBaHiA.

Rosman, P. C. C. (2018). Characteristic Hydraulic Times of the Jirau Hydropower Reservoir on the Madeira River - Braziliam Amazon Region. In: R. C. V. Silva, C. E. M. Tucci, C. A. Scott (Eds.), *Water and Climate - Modeling in large basins*. (pp. 95–132). [S.l.] Brazilian Water Resources Association.

Santos, E., Cunha, A., & Oliveira, E. (2014). Análise espaço-sazonal da qualidade da água na zona flúvio-marinha do Rio Araguari-Amazônia Oriental-Brasil. *Revista Brasileira de Recursos Hídricos*, *19*, 215–226. https://doi.org/10.21168/rbrh.v19n3.p215-226

Santos, E. S., & Cunha, A. C. (2021). Circulação secundária atípica de meandro fluviomarinho como parâmetro hidrodinâmico em ecossistema aquático amazônico. *Revista Ibero-americada de Ciências Ambientais*, *12*, 17. (In portuguese). https://10.6008/CBPC2179-6858.2021.003.0021

Scarano, F. R., Pereira, T. S., & Rôças, G. (2003). Seed germination during floatation and seedling growth of *Carapa guianensis*, a tree from flood-prone forests of the Amazon. *Plant Ecology*, *168*, 291–296. https://doi.org/10.1023/A:1024486715690

Schurr, F. M., Steinitz, O., & Nathan, R. (2008). Plant fecundity and seed dispersal in spatially heterogeneous environments: Models, mechanisms and estimation. *Journal of Ecology*, *96*, 628–641. https://doi.org/10.1111/j.1365-2745.2008.01371.x

Shaheed, R., Yan, X., & Mohammadian, A. (2021). Review and comparison of numerical simulations of secondary flow in river confluences. *Water*, *13*, 1917. https://doi.org/10.3390/w13141917

Shi, W., Shao, D., Gualtieri, C., Purnama, A., & Cui, B. (2020). Modelling long-distance floating seed dispersal in salt marsh tidal channels. *Ecohydrology*, *13*, e2157. https://doi.org/10.1002/eco.2157

Silva Dos Santos, E., Pinheiro Lopes, P. P., da Silva Pereira, H. H., de Oliveira Nascimento, O., Rennie, C. D., da Silveira Lobo O'Reilly Sternberg, L., & Cavalcanti da Cunha, A. (2018). The impact of channel capture on estuarine hydro-morphodynamics and water quality in the Amazon delta. *The Science of the Total Environment*, *624*, 887–899. https://doi.org/10.1016/j.scitotenv.2017.12.211

Silva, G. C. X., Medeiros de Abreu, C. H., Ward, N. D., Belúcio, L. P., Brito, D. C., Cunha, H. F. A., & da Cunha, A. C. (2020). Environmental impacts of dam reservoir filling in the East Amazon. *Frontiers in Water*, *2*, 11. https://doi.org/10.3389/frwa.2020.00011

Simonian, L. T. L., da Silva, J. B., de Andrade, R. F., & Almeida, A. C. P. C. (2003). Floresta Nacional do Amapá: Breve histórico, políticas públicas e (in)sustentabilidade.

Tagestad, J., Ward, N. D., Butman, D., & Stegen, J. (2021). Small streams dominate US tidal reaches and will be disproportionately impacted by sea-level rise. *Science of the Total Environment*, *753*, 141944. https://doi.org/10.1016/j.scitotenv.2020.141944

Targhetta, N., Kesselmeier, J., & Wittmann, F. (2015). Effects of the hydroedaphic gradient on tree species composition and aboveground wood biomass of oligotrophic forest ecosystems in the central Amazon basin. *Folia Geobotanica*, *50*, 185–205. https://doi.org/10.1007/s12224-015-9225-9

Ward, N. D., Keil, R. G., Medeiros, P. M., Brito, D. C., Cunha, A. C., Dittmar, T., Yager, P. L., Krusche, A. V., & Richey, J. E. (2013). Degradation of terrestrially derived macromolecules in the Amazon River. *Nature Geoscience*, *6*, 530–533. https://doi.org/10.1038/ngeo1817

Weber, L. J., Schumate, E. D., & Mawer, N. (2001). Experiments on flow at a 90° open-channel junction. *Journal of Hydraulic Engineering*, *127*, 340–350. https://doi.org/10.1061/(ASCE)0733-9429(2001)127:5(340)

Wittmann, F., Schöngart, J., Montero, J. C., Motzer, T., Junk, W. J., Piedade, M. T. F., Queiroz, H. L., & Worbes, M. (2006). Tree species composition and diversity gradients in white-water forests across the Amazon Basin. *Journal of Biogeography*, *33*, 1334–1347. https://doi.org/10.1111/j.1365-2699.2006.01495.x

SUPPORTING INFORMATION

Additional supporting information can be found online in the Supporting Information section at the end of this article.

How to cite this article: da Silva, E. B., Crizanto, J. L. P., de Abreu, C. H. M., dos Santos, E. S., Cunha, H. F. A., Brito, A. U., de Oliveira, G. P., Oliveira, L. L., Mortati, A. F., André, T., Schöngart, J., Piedade, M. T. F., & da Cunha, A. C. (2022). Experimentation, modelling, and simulation of hydrochory in an Amazonian river. *Freshwater Biology*, *00*, 1–14. https://doi.org/10.1111/fwb.14015